New Network Permeability Model of Porous Media

In this study a new mathematical model for predicting permeabilities of porous media has been developed. The model consists of a set of cubic networks of arbitrary orientations with respect to the macroscopic flow direction. The networks consist of capillary tubes which are made up of segments of different diameters. It is shown that a cubic network of capillaries has isotropic permeability properties. The permeability model requires two pore size distributions and the porosity of the sample for the calculations. The calculated permeabilities agreed with experimental results for a wide range of permeabilities of highly compacted materials to within ± 23%, without using adjustable tortuosity factors.

FRANCIS A. L. DULLIEN

Institut fur Mechanische Verfahrenstechnik
Universitat Karlsruhe, Germany

SCOPE

The importance of porous media in a large variety of engineering endeavors is widely appreciated. Modeling the transport properties of porous media is a formidable task because of the great complexity of pore structure. The existing models of permeability are often inadequate, particularly for highly compacted porous media. In the present study an improved equation has been developed to calculate permeabilities of a large variety of porous media using easily obtainable pore structure data.

The main deficiencies of existing mathematical models of porous media are due to insufficient information on pore structure. A great deal of experimental data show that there exist continuous flow capillaries of different effective diameters in porous media and that the effective cross section varies in a quasi periodic manner along the length of each capillary. It is shown in this study that a mean hydraulic pore diameter cannot account for variations in these structural characteristics. Use of the customary distribution of pore entry diameters without taking into account the size of the pores penetrated through the entry pores is shown to result in absurd conclusions on the pore structure.

A mathematical model of permeability has been developed in this study which takes into account certain important features of the actual pore structure that have been unaccounted for in previous models. The experimental basis for the model consists of characterization of the flow capillaries by using two pore size parameters: the controlling pore entry diameter and the diameter of all the other pore segments which may be penetrated through the controlling neck. For some samples this bivariate distribution has been determined experimentally. For some others it has been estimated using the mercury intrusion porosimetry curve and the photomicrographic pore size distribution curve of the sample. By measuring the permeability of evacuated samples to mercury at different saturations with mercury, it has been shown that there are continuous flow paths in homogeneous porous media which are controlled by the largest pore entry diameters.

The permeability model consists of a set of three-dimensional cubic capillary networks with arbitrary orientations with respect to the macroscopic flow direction. The various networks are characterized by different pore entry diameters, different distributions of pore diameters, and different cell constants. Each network is assumed to be built up of identical capillary tubes which, however, are different in the various networks. Each capillary is made up of segments of different diameters.

CONCLUSIONS AND SIGNIFICANCE

It has been proven in this study that a three-dimensional cubic network of capillaries has isotropic permeability. A formula has been derived on the basis of the model to calculate sample permeabilities using pore size distributions and porosities. The theoretical equation contains a constant numerical factor of 96. Permeabilities have been calculated by this equation and compared with experimental values for fourteen widely different samples. The permeabilities have ranged over five orders of magnitude. Good general agreement between the calculated and experimental permeabilities has been found. The best fit to the data requires the constant 96 to be replaced by the empirical value of 106. Using this value the calculated permeabilities agreed with the experimental values within ± 23%. This agreement with experiments is far better than any existing permeability model would have been able to provide. The fact that there was no need to use arbitrary tortuosity factors in order to have agreement is particularly significant. The numerical coefficient 106 may be interpreted as corresponding to a constant tortuosity factor equal to 3.3, whereas the theoretical value corresponding to the model is equal to 3. Further improvement of the model is possible which should have the result of reducing the value of the empirical constant 106.

The permeability model given here makes it possible to calculate permeabilities of a large variety of porous media from two pore size distribution functions and porosities. Its success is due to a better appreciation of pore structure.

F. A. L. Dullien is with the University of Waterloo, Waterloo, Ontario, Canada.

Mathematical models of porous media have a very extensive literature (for example, Scheidegger, 1963; Bear, 1972) a detailed review of which is outside the scope of this paper.

MAIN DEFICIENCIES OF EXISTING MODELS

In the case of existing mathematical models the information on pore structure is limited to the bulk porosity ϵ, and either the mean hydraulic pore diameter D_H or the distribution of pore entry diameters obtained from a drainage capillary pressure or mercury intrusion porosimetry curve. In the first case all the pores in the model have the same diameter which is far from reality for most real porous media, whereas in the second case only the entry pore diameters are used and the volume of the other pores is assigned to the entry diameters.

The widely used Carman-Kozeny permeability equation (for example, Scheidegger, 1963; Bear, 1972) is as follows:

$$k_{CK} = \frac{\epsilon D_H^2}{16\, k'} \tag{1}$$

where

$$D_H = \frac{4\epsilon}{S(1-\epsilon)} \tag{2}$$

is the channel diameter, equal to 4 times the hydraulic radius, and S is the specific surface area of the solids in the medium. $k' = k_0(L_e/L)^2$ is the "Kozeny constant", where k_0 has been called *shape factor* by Carman and given the value 2.5, and $(L_e/L)^2$ is the *tortuosity factor* to which Carman assigned the value 2.0.

The Carman-Kozeny equation with $k' = 5$ is often a reasonable approximation, particularly in the case of unconsolidated media. Nevertheless, k' is not a true constant and there have been many cases where very great deviations from the Carman-Kozeny equation have been observed.

In a series of careful measurements Rumpf and Gupte (1971) have shown that even for randomly packed beds consisting of a narrow distribution of spheres, k' varies with the porosity. For $\epsilon = 0.35$ they found $k' = 5.1$; at $\epsilon = 0.55$ they had $k' = 3.4$, and at $\epsilon = 0.75$ they obtained again $k' = 5.1$, indicating that with increasing ϵ there is first a decrease, followed by an increase in the value of k'. For fibrous structures of porosities $\epsilon = 0.85$ and more increasingly high values of k' are required to obtain agreement with experiments (Wasan et al., 1970).

It is evident from Equations (1) and (2) that, for constant k', the value of k_{CK} is uniquely determined by the porosity ϵ and the specific surface area S. It is easy to demonstrate, however, that the permeability depends also on the distribution and the topographical arrangement of capillaries of different diameters. Analogously, as is the case in electric circuits, capillaries of different conductivities also may be either in parallel or in series connection.

PARALLEL TYPE NONUNIFORMITIES

The existence of continuous flow channels of different diameters, leading from one face of the sample to the other has been demonstrated experimentally by Hewitt (1967) and Batra (1973), and by model calculations on random packs, by Schubert (1971).

For simplicity, assuming a bundle consisting only of 2 different sizes of cylindrical capillaries of diameters D_l (l = large) and D_s (s = small), respectively, and equal length, it can be readily shown by using the Hagen-Poiseuille equation for each capillary that the bundle permeability k varies as

$$k = k_{CK}\frac{(1+yx^4)(1+yx)^2}{(1+yx^2)^3} \tag{3}$$

with $x = D_l/D_s$ and $y = \nu_l/\nu_s$ is the number ratio of large-to-small capillaries. k_{CK} is the value of the permeability calculated by Equation (1) using $k' = 2$ which is the appropriate value for straight cylindrical capillaries. Equation (3) yields for example, for $x = 3$ and $y = 0.1$, $k = 2.24\, k_{CK}$. It can be readily shown that the effect of parallel type nonuniformities always is a higher actual permeability than the value predicted by using a mean hydraulic pore diameter. It is noted that this effect necessitates the use of lower values of k' (that is, of $(L_e/L)^2$) in Equation (1) in order to be in agreement with experimental facts. The value of k' which is needed for agreement with the experiments may be even less than unity. It was pointed out a long time ago (Childs and Collis-George, 1950) that the Carman-Kozeny model fails completely in the case of structured bodies containing fissures. For example, for $x = 10^3$ and $y = 10^{-6}$, Equation (3) yields $k = 10^5\, k_{CK}$.

SERIAL TYPE NONUNIFORMITIES

In addition to the parallel type pore nonuniformities discussed above, the effective cross section of capillaries in porous bodies is known to vary in a quasiperiodic manner (for example, Haines, 1930; Smith, 1932; Dullien et al., 1972; Dullien and Batra, 1973; Dullien and Dhawan, 1974).

For simplicity, assuming a bundle of identical straight cylindrical capillaries, each consisting of a sequence of wide and narrow segments of diameters D_l and D_s, it can be readily shown by use of the Hagen-Poiseuille equation for each segment, neglecting expansion and contraction losses, that the bundle permeability k varies as

$$k = k_{CK}\frac{(1+y)^2(1+yx)^2}{(1+yx^2)^3(1+y/x^4)} \tag{4}$$

with $x = D_l/D_s$ and $y = l_l/l_s$, where l_l and l_s are the aggregate lengths of the wide and narrow portions, respectively. For example, with $x = y = 2$ Equation (4) yields $k = 0.27\, k_{CK}$, where k_{CK} is calculated by Equation (1) using $k' = 2$. The effect of serial type nonuniformities, demonstrated by the above example, is for all practical values of x and y to make the actual permeability smaller than k_{CK}.

It is evident that the effects of the parallel and serial type nonuniformities are of opposite sense, and therefore there is a possibility for mutual cancellation of the two effects.

USE OF PORE ENTRY DIAMETER DISTRIBUTIONS

Turning now to the use of the distribution of pore entry diameters, as shown in Figure 1, this approach results in unrealistic pore model. In the figure, for purposes of illustration, two pore sizes are assumed: the small pore diameter D_s is the pore entry diameter and the large pore diameter D_l is the diameter of the other pores. As a typical value, it is assumed that $D_l/D_s = 3$. It is also assumed that all the pores are cylindrical and that the length of the small pores is equal to the length of the large pores. Bearing in mind that mercury intrusion porosimetry and the drainage branch of the capillary pressure curve give absolutely no information on the size or even the existence of the large pores, it will appear to the investigator that all pores have the diameter D_s. At the same time, the investigator measures the total pore volume which is equal to $(D_l^2 + D_s^2)\,\pi/4$. Assigning all this volume to the capillaries of diameter D_s he concludes that there are five

capillaries of diameter D_s in parallel instead of the one capillary actually present. The above illustration is, of course, quite oversimplified, but it serves the purpose of making the point that mathematical models which pretend that all pores are entry pores lead to absurd conclusions on the pore structure.

EXPERIMENTAL BASIS OF PERMEABILITY MODEL

The objective of this work has been to develop a mathematical model of pore network which takes into account certain important features of actual pore structure unaccounted for in previous models. New information on pore structure has been obtained in a series of experimental projects.

Entry Pore Size Distribution vs. Actual Pore Size Distribution

In one of the experimental projects the distribution of pore volume of a large number of porous samples has been determined by two methods: mercury porosimetry and quantitative photomicrography. The latter method gives the distribution of pore volume by all pore diameters D, and therefore it is much closer to reality than the entry diameter D_e distribution obtained by mercury intrusion

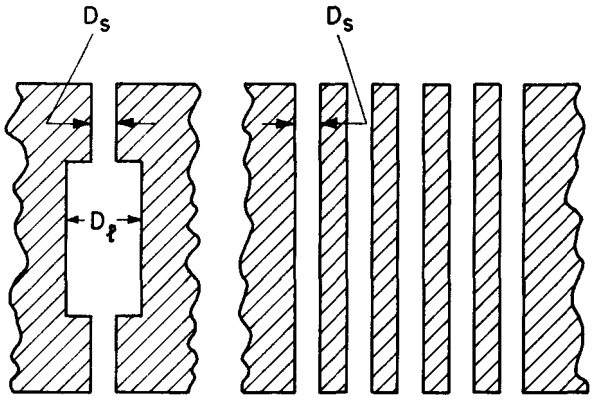

Fig. 1. Effect of using pore entry diameters.

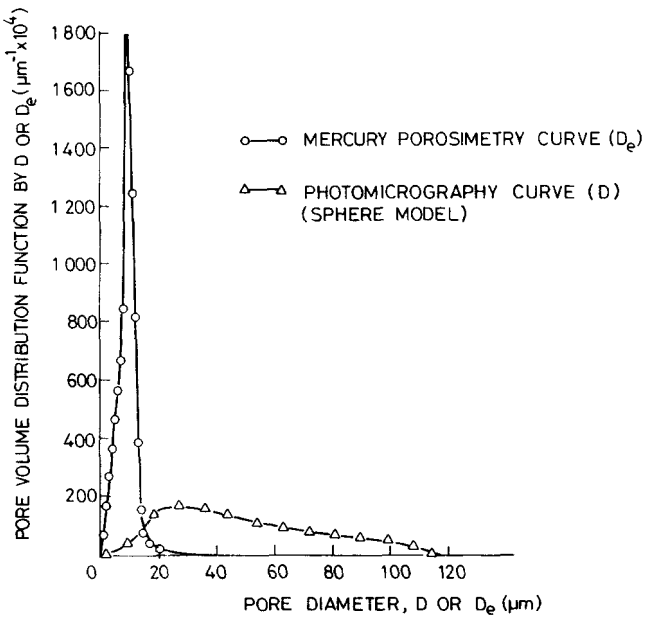

Fig. 2. Comparison of pore volume distributions for a sandstone (Big Clifty 140).

porosimetry. A typical example is shown in Figure 2 where the two distributions obtained on a sandstone sample are compared with each other. The assumptions made and techniques used in the quantitative photomicrographic method have been discussed in a series of publications (Dullien and Dhawan, 1973; Dullien and Batra, 1970; Dullien and Dhawan, 1974; Dullien and Mehta, 1971/72). It is evident from Figure 2 that the difference between the two distributions is very great. As this is typical of most porous media, a realistic mathematical model of the pore network must take it into account.

Pore Volume Distribution by Two Pore Size Parameters

In another experimental project, the relationship between pore entry diameters D_e and the diameters D and volumes of the pore segments which are accessible through D_e has been determined for some samples. This work which has been described in detail by Dullien and Dhawan (in press) has resulted in bivariate pore volume distributions, $\alpha(D_e, D)\, dD_e dD$, giving the fraction of pore volume which is accessible to the non-wetting phase through controlling necks (entry pores) in the diameter range $D_e \rightarrow D_e + dD_e$ and that have diameters in the range of $D \rightarrow D + dD$.

Because of the very time consuming nature of these determinations, a technique has been devised to estimate the bivariate distribution function for samples where only the two pore size distribution curves exemplified in Figure 2 were available.

The bivariate distribution can be conveniently presented in the form of a two-dimensional histogram (see Figure 3.b). In the matrix, index i denotes pore of entry and index j denotes any pore, D_i is pore entry diameter, and D_j is diameter of any pore. V_{ij} is the percent pore volume in the sample associated with diameters D_i and D_j. Since the largest pore of entry in the sample is penetrated first, that is to say, at the lowest value of the capillary pressure, the matrix in Figure 3 is best read starting with the entry in the lower left corner. Proceeding to the right, the percentage pore volumes of the various pore segments are tabulated which were penetrated through the largest pore of entry, corresponding to $i = 3$, and $D_i = 15.5\ \mu$. Evidently, the smallest possible value of j is equal to i in every row. The entries in the matrix corresponding to $i = j$ give the percentage pore volumes occupied by the pores of entry. It is apparent from the table that these volumes make up only a very small percentage of the total pore volume of the sample.

The calculation of the bivariate pore volume distribution was done as follows: The area under the mercury porosimetry curve (see Figure 2) was divided into three parts of equal area. For very narrow mercury porosimetry peaks two and for the broadest peaks four subdivisions were used. The lower boundary of each zone represents the diameter of the smallest pore penetrated in the pore volume represented by the entire area under the curve to the right of the boundary. As shown in Figure 3a, for each zone a curve similar to the experimental photomicrographic pore size distribution curve (Figure 2) was drawn such that the area under the curve was proportional to the pore volume penetrated. From the curves in Figure 3a, the bivariate pore volume distribution was calculated by subdividing the whole diameter range into suitable increments and calculating the areas of the zones lying between adjacent curves within these increments, as exemplified by the cross-hatched area in Figure 3b.

An important conclusion may be drawn from the results obtained in these experiments: large as well as small pores are entered through small pores of entry. In other words, these results do not confirm the assumption (Payatakes et

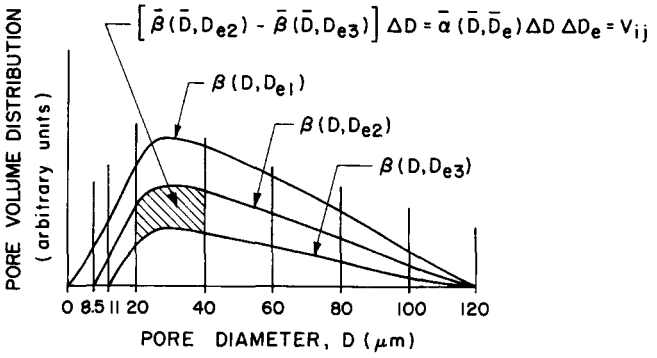

a) CALCULATION SCHEME

	i \ j	1	2	3	4	5	6	7	8	D_i
V_{ij}	1	0.8	1.0	3.9	9.2	8.1	6.4	4.3	1.4	4.25
	2	0	0.3	3.4	9.3	8.6	6.6	3.1	1.0	9.75
	3	0	0	1.5	10	8.6	6.0	4.3	1.9	15.5
	D_j	4.25	9.75	15.5	30	50	70	90	110	

b) THE RESULT: BIVARIATE PORE VOLUME DISTRIBUTION

Fig. 3. Calculation of the coefficients V_{ij} from the pore size distributions shown in Figure 2.

al., 1973) according to which small pore necks are preferentially adjoining small pore bulges and conversely large pore necks lead into large pore bulges. This is probably the case only when comparing different packed beds each consisting of practically monosized particles. The bed consisting of the smaller particles will tend to contain smaller bulges as well as smaller necks, on the average, than the bed made up of larger particles.

Permeability to Mercury vs. Saturation with Respect to Mercury

In a third experimental project, the contribution to the permeability by the pores represented in the different rows of the matrix similar to the one shown in Figure 3 was measured for a large number of samples. The apparatus used for this purpose was designed after that of Hewitt (1967) and is shown diagramatically in Figure 4. This kind of equipment is called *mercury permeameter* and the technique employing this equipment is known as *mercury permeametry*.

The objective of mercury pereametry is to measure the permeability of the evacuated sample to mercury at different saturations with mercury. This technique is similar to the customary relative permeability measurements using water, and oil or gas, but it is devoid of the complicating effects caused by the presence of a viscous and incompressible wetting phase.

The unit built and used in this study (Batra, 1973) is operated as follows: After raising the mercury level just above valve V13, both sides of the system are evacuated. After shutting valve V7, and opening valves V12 and V13, mercury is permitted to rise in both manometer tubes. At the same time, both faces of the sample are flooded with mercury.

For measurements at subatmospheric pressures, some air is let into the system by opening valve V2 for a short time, after shutting valve V1. The level of mercury is permitted to fall in G2 and rise in G1 by a small amount. After shutting valve V12 and opening V1, both sides of the system are again evacuated. The height difference of mercury in the two manometer tubes makes the mercury flow through the sample. The change of height of mercury in the manometer tubes is automatically recorded by the use of resistance wires in the tubes.

For measurements made above atmospheric pressure, nitrogen gas is admitted to the two sides from two separate cylinders until the desired pressure is reached, in such a manner that the mercury is at the same level in the two manometer tubes. After the penetration of mercury into the sample reaches equilibrium, a small pressure differential is set up by opening V10 for a short time. As a result, mercury starts flowing through the sample from G1 to G2. The change in height in the tubes is recorded automatically vs. time.

The pressure is raised in a stepwise manner from run to run until the sample is completely saturated with mercury and no more increase in permeability can be registered. In each run the permeability is calculated in the customary manner from the variation with time of the mercury levels in the manometer tubes (Batra, 1973). The saturations with respect to mercury at the various pressures are taken from the mercury porosimetry curve of the sample.

Typical mercury permeability vs. saturation curves are shown in Figure 5. It is evident from the curves that already at a relatively low saturation there must be continuous flow channels in the medium which contribute a significant fraction of the total permeability. At the low saturations only the largest entry pores in the sample are penetrated by the mercury; therefore, these flow channels consist only of such pores that can be penetrated through large pore necks.

From a hypothesis of random arrangement of pore segments of different diameters at first sight it may appear that pores of all different diameters should occur along each continuous path. In fact there are continuous paths in

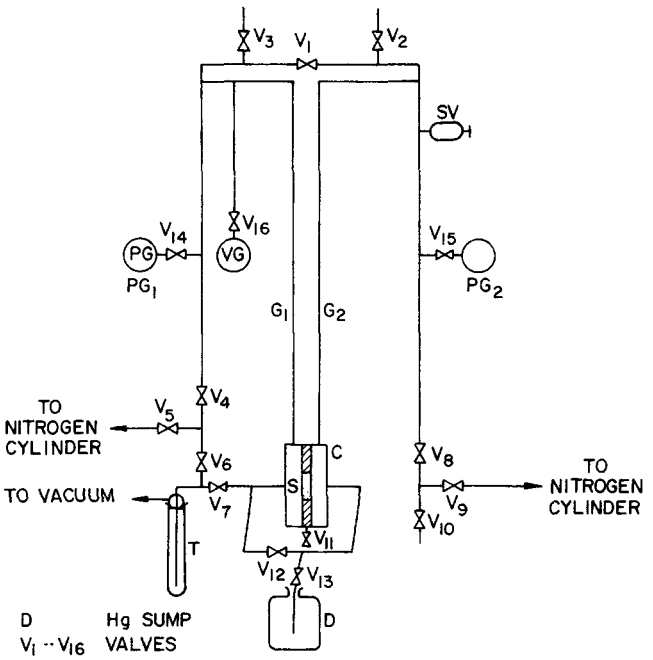

Fig. 4. Schematic diagram of mercury permeameter (Batra, 1973).

the medium which contain only the largest pore segments. This is a very important fact since such a channel has much higher hydraulic conductivity than one of equal length containing the complete distribution of pore diameters. Therefore, these channels play a very significant role in the sample permeability.

This behavior is not necessarily a consequence of nonrandom pore structure, and therefore it should be distinguished from the phenomenon commonly called *channeling*. Schubert (1971) has shown by model calculations that breakthrough to a nonwetting phase from the inlet to the outlet face of a system containing random distribution of 10 different pore diameters, arranged on a square lattice, occurs after the penetration of the third largest pore diameter (number 8 on a scale of 10-1). Hence even for completely random arrangement of pore diameters, there are continuous paths across the sample which contain only the largest pore diameters. There follows that a certain degree of channeling is unavoidable even in the case of ideally random packing.

In Figure 5 the observed increase in permeability with saturation is the result of penetration of mercury into increasingly narrow pore necks. Additional flow channels, characterized by decreasing values of D_i (Figure 3) become thus filled with mercury and contribute to the flow across the sample. It is noted that each new path is of necessity in parallel connection with some existing flow channels and may or may not be in series connection with some others. If a new flow channel runs from one face of the sample to the other without intersecting any of the already contributing channels then it will not be in series connection with any of them. In Figure 6, the various possibilities are shown diagramatically.

THE PERMEABILITY MODEL

A realistic mathematical model of the pore network must take into account all of the above findings. Since the hydraulic conductivity of a flow channel is most sensitive to the diameter of the narrowest segment contained in it, the different flow paths must be characterized first of all by the smallest diameter they contain, that is, D_i. Since the other pore segments contained in a flow capillary, particularly those which are not very much greater than the entry pore also have an effect on its hydraulic conductivity, each flow channel should be characterized also by all the other segment diameters D_j. The relative aggregate lengths of the segments of different diameters contained in each flow channel are determined by the total volume V_{ij} of the various segments. It is evident that all the information necessary to calculate these properties of flow channels of the model are contained in the rows of the matrix in Figure 3b. Each row represents a different class i of flow channels.

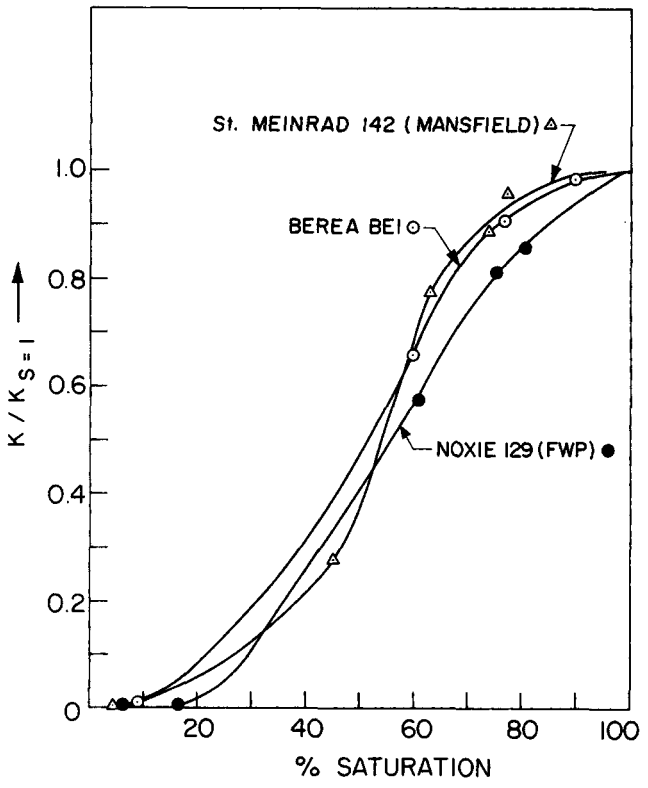

Fig. 5. Mercury permeability versus saturation curves for three different sandstones (Batra, 1973).

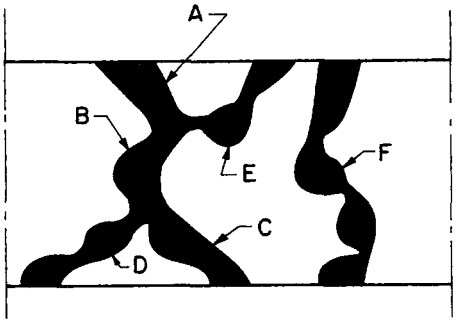

ABC : CAPILLARY CONTROLLED BY LARGE NECKS

D, E, and F : CAPILLARIES CONTROLLED BY NARROWER NECKS

ABC IS IN PARALLEL CONNECTION WITH F ;

D IS IN PARALLEL CONNECTION WITH C ;

E IS IN PARALLEL CONNECTION WITH A ;

D and E ARE IN SERIES CONNECTION WITH B

Fig. 6. Parallel and series arrangements of flow channels controlled by necks of different diameters.

Definition of Model

The facts on pore structure which are available as a result of the above experimental work permit a number of possible arrangements of the flow capillaries. The information available on pore structure defines the various classes i of capillaries with respect to the size distribution and relative lengths of the pore segments contained in them. One might think of a set of different strings of beads, each with a given distribution of bead sizes and total string length. The problem is how to arrange these strings of beads in a box. For example, one could cut each string into representative parts of equal length equal to the distance between the two faces of the box and form a parallel bundle of them. This model would be extremely anisotropic because it would have permeability only in the direction parallel to the bundle and zero permeability in all other directions. In addition, a bundle does not have network properties whereas real porous media do. It is important to have network characteristics and isotropic properties incorporated in the model. It is equally important that the model could be readily used for numerical calculations.

The permeability model consists of a set of three-dimensional networks. Each class i of flow capillaries forms an independent network in the model. A network i is assumed to be built up of identical capillary elements. Using once more the analogy of a string of beads, imagine that the

beads are arranged on the string in such a way that the various sized beads repeat periodically as shown diagramatically, using five different pore segments, in Figure 7. Then the string is cut into pieces so as to obtain identical short strings of beads. These pieces are used as capillary elements of the network. Each element has the same length, the same size distribution, and the same hydraulic conductivity. The elements in the different classes i of networks have different size distributions, lengths, and hydraulic conductivities.

The independence of the different networks i, corresponding to the different classes i, is an assumption. In reality the flow capillaries of the different classes i most likely intersect with each other. It is possible, however, that the intersections don't make a major difference in permeability for the reason shown diagramatically in Figure 8. As is apparent from this figure, the pressure in the two capillaries of different diameters is the same at the mathematical point of intersection and, therefore, in the case of actual intersection it will not change its value. Thus the flow rates will remain unchanged, too. The hydrodynamic disturbance at the point of intersection has been neglected in this simple argument, and the two capillaries have been treated as two electric conductors.

For the present mathematical model, a cubic network of the capillary elements has been chosen with an arbitrary orientation with respect to the macroscopic flow direction. As it will be shown below, a cubic network of capillaries is isotropic; in other words, it has the same permeability in any arbitrary direction as the permeability measured in any one of the principal directions. Using the cubic lattice

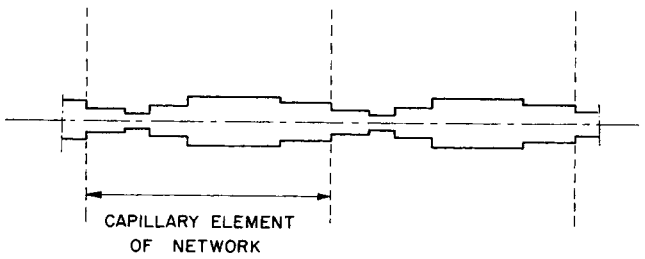

Fig. 7. Schematic diagram showing capillary element of which cubic lattice is built.

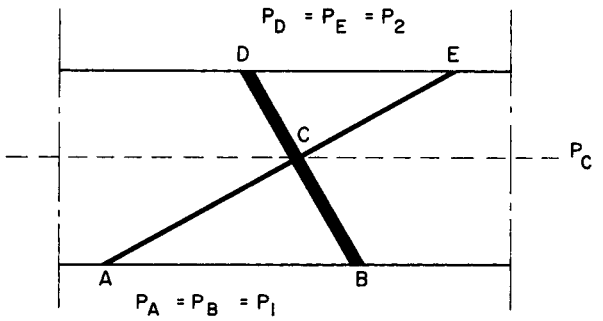

Fig. 8. Pressure distributions in two intersecting capillaries of different diameters.

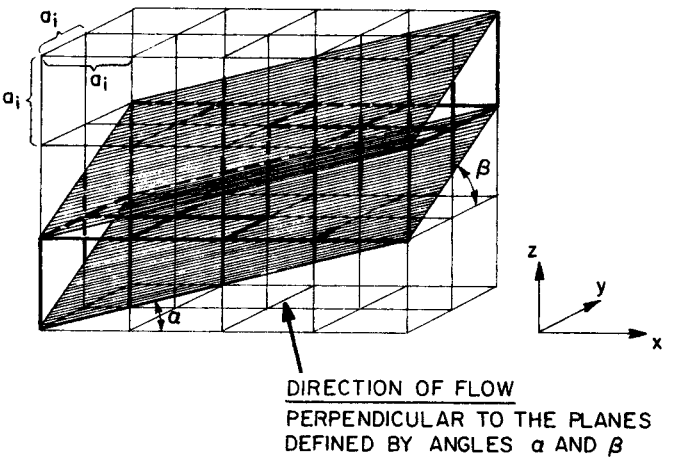

Fig. 9. Representative cell of model—the capillaries drawn in heavy lines are contained in the cell between the two parallel planes.

oriented with one of the principal directions parallel to the macroscopic flow direction is not satisfactory because only one-third of the capillaries are conducting, the other two-thirds, however, contain stagnant fluid. Using the cubic lattice in an arbitrary orientation with respect to the flow direction, however, appears to amount to a reasonable network model.

A representative element of arbitrary orientation cut out of the cubic lattice by two parallel planes is shown diagramatically in Figure 9. The orientation of the planes is defined by the two angles α and β. The two planes should be thought of as having infinite extent; however, the finite cell shown in the figure, as used in the calculations below, is representative of the region contained between the two infinite planes.

Calculation of Permeability of Model

In the following the permeability of the representative unit cell will be calculated. The different classes of flow capillaries in the model will in general have different cell constants a_i and, of course, also different permeabilities k_i. The treatment below is given for class i of flow capillary.

First the volumetric flow rate across the two faces perpendicular to the macroscopic flow direction of the i-cell will be calculated. In the i-cell, the lengths of the x-, y-, and z-tubes are, respectively,

$$(l_i)_x = a_i \cot\alpha$$
$$(l_i)_y = a_i \cot\beta \qquad (5)$$
$$(l_i)_z = a_i$$

The numbers of x-, y-, and z-tubes in the cell are, respectively,

$$n_x = \cot\beta$$
$$n_y = \cot\alpha \qquad (6)$$
$$n_z = \cot\alpha \cot\beta$$

The volumetric flow rate in the cell is

$$Q_i = (Q_i)_x + (Q_i)_y + (Q_i)_z \qquad (7)$$

where $(Q_i)_x$, $(Q_i)_y$, and $(Q_i)_z$ are the volumetric flow rates in the cell contributed by all the x, y, and z tubes, respectively. Assuming laminar flow and neglecting contraction and expansion losses, these flow rates can be expressed by using the Hagen-Poiseuille equation for arbitrary capillary j-segments in the flow capillaries as follows:

$$(Q_i)_x = \frac{(\Delta P_{ij})_x}{l_{ij}} \frac{D_j^4 \pi}{128\,\mu} \cot\beta$$

$$(Q_i)_y = \frac{(\Delta P_{ij})_y}{l_{ij}} \frac{D_j^4 \pi}{128 \mu} \cot \alpha \tag{8}$$

$$(Q_i)_z = \frac{(\Delta P_{ij})_z}{l_{ij}} \frac{D_j^4 \pi}{128 \mu} \cot \alpha \cot \beta$$

where ΔP_{ij} is the pressure drop in a segment of length l_{ij}. Let the total number of l_{ij} segments in the cell be n_{ij}. Thus the total length of these segments in the cell is $n_{ij} l_{ij}$, and the total length of flow capillaries contained in the cell is

$$L_i = \sum_j n_{ij} l_{ij} \tag{9}$$

However, this length can also be expressed by using Equations (5) and (6) as follows:

$$L_i = a_i \cot \alpha \cot \beta + a_i \cot \alpha \cot \beta + a_i \cot \alpha \cot \beta$$

$$= 3a_i \cot \alpha \cot \beta \tag{10}$$

Thus

$$\sum_j n_{ij} l_{ij} = 3a_i \cot \alpha \cot \beta \tag{11}$$

The $\cot \beta$ x-tubes make up 1/3 of the total tube length. Thus the number of l_{ij} segments in one x-tube is $n_{ij}/3 \cot \beta$. The number of l_{ij} segments in all the y-tubes and z-tubes is also $n_{ij}/3$. Hence the number of l_{ij} segments in one y-tube is $n_{ij}/3 \cot \alpha$ and in one z-tube $n_{ij}/3 \cot \alpha \cot \beta$.

Since the pressure gradients are inversely proportional to the tube lengths

$$(\Delta P_{ij})_x (n_{ij}/3 \cot \beta) = (\Delta P_{ij})_y (n_{ij}/3 \cot \alpha) \tag{12}$$

or

$$\frac{(\Delta P_{ij})_y}{(\Delta P_{ij})_x} = \cot \alpha / \cot \beta \tag{13}$$

Analogously

$$\frac{(\Delta P_{ij})_z}{(\Delta P_{ij})_x} = \cot \alpha \tag{13b}$$

Combining Equations (13) with Equations (8) and substituting in Equation (7) there follows:

$$Q_i = (Q_i)_x (1 + \cot^2 \alpha / \cot^2 \beta + \cot^2 \alpha) \tag{14}$$

In the following sequence of manipulations, $(Q_i)_x$ is expressed in terms of the pressure drop ΔP between the faces of the unit cell. ΔP can be written as follows:

$$\Delta P = \sum_j (\Delta P_{ij})_x n_{ij}/3 \cot \beta \tag{15}$$

Introducing into Equation (15) the first Equation (8)

$$\Delta P = \frac{128 \mu (Q_i)_x}{3 \pi \cot^2 \beta} \sum_j n_{ij} l_{ij}/D_j^4 \tag{16}$$

Dividing the first Equation (8) by Equation (16):

$$\frac{(\Delta P_{ij})_x}{3 \Delta P \cot \beta} = \frac{l_{ij}/D_j^4}{\sum_j n_{ij} l_{ij}/D_j^4} \tag{17}$$

Substituting this result back into the first Equation (8)

$$(Q_i)_x = \frac{\Delta P \cot^2 \beta}{\sum_j n_{ij} l_{ij}/D_j^4} \frac{3 \pi}{128 \mu} \tag{18}$$

Introducing this expression for $(Q_i)_x$ into Equation (14) gives

$$Q_i = \frac{\Delta P}{\sum_j n_{ij} l_{ij}/D_j^4} \frac{3\pi}{128 \mu} (\cot^2 \alpha + \cot^2 \beta + \cot^2 \alpha \cot^2 \beta) \tag{19}$$

According to Darcy's law, the permeability k_i of the i-cell is

$$k_i = \frac{Q_i \mu}{A_i (\Delta P / L_i)} \tag{20}$$

where A_i, the cross-sectional area of the cell, is

$$A_i = a_i^2 \sqrt{\cot^2 \alpha \cot^2 \beta + \cot^2 \alpha + \cot^2 \beta} \tag{21}$$

and L_i, the distance between the two faces of the cell is

$$L_i = \frac{a_i \cot \alpha \cot \beta}{\sqrt{\cot^2 \alpha \cot^2 \beta + \cot^2 \alpha + \cot^2 \beta}} \tag{22}$$

A combination of Equations (19), (20), (21), and (22) results in

$$k_i = \frac{3 \pi \cot \alpha \cot \beta}{128 a_i \sum_j n_{ij} l_{ij}/D_j^4} \tag{23}$$

The total volume V_{ij} of all l_{ij} segments in the i-cell is

$$V_{ij} = \frac{D_j^2 \pi}{4} n_{ij} l_{ij} \tag{24}$$

From Equation (24) there follows:

$$\sum_j n_{ij} l_{ij}/D_j^4 = \frac{4}{\pi} \sum_j V_{ij}/D_j^6 \tag{25}$$

and also

$$\sum_j n_{ij} l_{ij} = \frac{4}{\pi} \sum_j V_{ij}/D_j^2 \tag{26}$$

Combining Equation (26) with Equation (11)

$$3 \cot \alpha \cot \beta = \frac{4}{\pi} \frac{\sum_j V_{ij}/D_j^2}{a_i} \tag{27}$$

The porosity ϵ_i of the i-cell is

$$\epsilon_i = \frac{\sum_j V_{ij}}{L_i A_i} = \frac{\sum_j V_{ij}}{a_i^3 \cot \alpha \cot \beta} \tag{28}$$

where Equations (21) and (22) have been used. Combination of Equations (23), (25), (27), and (28) results in

$$k_i = \frac{\epsilon_i}{3 \times 32} \frac{(\sum_j V_{ij}/D_j^2)^2}{(\sum_j V_{ij})(\sum_j V_{ij}/D_j^6)} \tag{29}$$

It is important to note at this point that the result expressed in Equation (29) implies that the permeability of a cubic network of capillaries is independent of the macroscopic flow direction through the network. As shown in a separate communication (Dullien, to be published), this result holds independently of the bivariate pore volume distribution also used in the model. It is only necessary that the tubes of which the cubes consist should either all have the same conductivity or the conductivities be distributed randomly over the whole network. The permeability of all such cubic networks is isotropic. It can also be shown that anisotropy can be modeled by using either capillaries of three different conductivities or three different cell constants (a_i, b_i, c_i) in the three principal directions of the network.

Evidently

$$\frac{\epsilon_i}{\sum_j V_{ij}} = \frac{\epsilon}{\sum_i \sum_j V_{ij}} \tag{30}$$

where ϵ is the total bulk porosity and $\sum_i \sum_j V_{ij}$ is the total pore volume of the sample. Using Equation (30) in Equa-

tion (29) gives the final expression for the permeability k_i of the i-cell

$$k_i = \frac{\epsilon}{96 \sum_i \sum_j V_{ij}} \frac{(\sum_j V_{ij}/D_j)^2}{\sum_j V_{ij}/D_j^6} \tag{31}$$

In the model, the assumption of independent networks has been made for different values of i, and hence, the permeabilities k_i of the i-networks are additive, resulting in the expression for total permeability k_m of the model

$$k_m = \sum_i k_i \tag{32}$$

The form of Equation (31) is similar to that of all geometric permeability models including, of course, the Carman-Kozeny model [compare with Equation (1)]. The value of the constant in the denominator of Equation (31) is equal to 96 a fact which, in harmony with independent results (Satterfield, 1970; Haring and Greenkorn, 1970), may be interpreted as a tortuosity factor of 3 for the model. The part of Equation (31) consisting of the three summations is merely the value of the mean square diameter $\overline{D_i^2}$ of the flow channel i according to the present model; therefore Equation (32) may be written as

$$k_m = \frac{\epsilon}{96} \sum_i \overline{D_i^2} \tag{33}$$

RESULTS AND DISCUSSION

The mathematical model has been tested by evaluating k_m using Equation (33) and comparing the result with the measured permeability k in the case of 14 widely different sandstones. The reason for using sandstones was partly an appreciation of the well-known difficulties which have been experienced in the past by other workers when trying to predict sandstone permeabilities by using other models, partly the fact that a great deal of work had been done on these sandstones in these laboratories, and therefore they were available and it was logical to use them also for testing the permeability model.

The permeabilities of the sandstones were measured by Dhawan (1972) and Batra (1973) by flowing 2% NaCl solutions through the samples and were remeasured for ten of the sandstones by Azzam (1974) using unsteady state gas permeametry over a wide range of flow rates. Details of this latter work will be reported in another communication. Whenever available, the more extensive measurements of Azzam were used for comparison with the calculated permeabilities. The porosities were determined gravimetrically by saturating the samples with 2% NaCl solution.

For two of the sandstones, Bartlesville and Berea (BE-1), the bivariate pore size distribution function was determined by Woods Metal Porosimetry by Dhawan (1972), (also Dullien and Dhawan, 1974, in press). As the experimental labor involved in this work is very tedious, for the rest of the samples, the bivariate pore volume distribution function was estimated from the two different pore size distribution curves which were determined for each sample (see Figures 2 and 3) by using the technique described above in the experimental part of this paper.

A comparison of the permeabilities k_m calculated by Equation (33) with the experimental values k_{exp} has shown that the former were on the average about 10% too high, that is, the experimental permeabilities were, in the mean, better fitted by the calculated permeabilities k_{calc} obtained by the equation

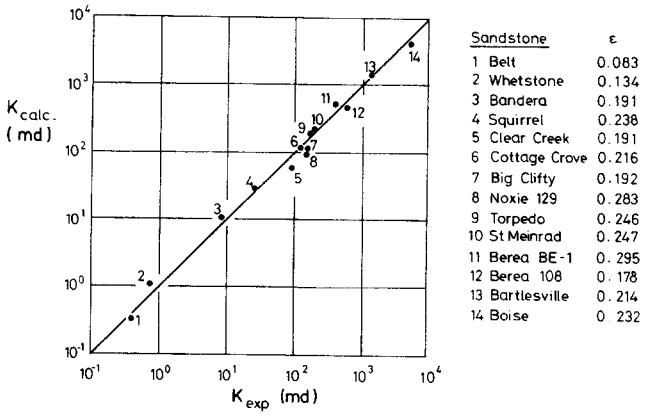

Sandstone	ε
1 Belt	0.083
2 Whetstone	0.134
3 Bandera	0.191
4 Squirrel	0.238
5 Clear Creek	0.191
6 Cottage Grove	0.216
7 Big Clifty	0.192
8 Noxie 129	0.283
9 Torpedo	0.246
10 St Meinrad	0.247
11 Berea BE-1	0.295
12 Berea 108	0.178
13 Bartlesville	0.214
14 Boise	0.232

Fig. 10. Comparison of calculated vs. experimental permeabilities of sandstones.

$$k_{calc} = \frac{\epsilon}{106} \sum_i \overline{D_i^2} \tag{34}$$

The permeabilities k_{calc} calculated by Equation (34) are compared with the experimental values k_{exp} in Figure 10. As it is apparent from this figure, the permeabilities of the sandstones covered in this study range over five cycles. All the points on the graph are within a factor of 1.7 from the 45° line, 86% of them are within a factor of 1.4 and 43% are within a factor of 1.2. The average scatter of the points about the 45° line ± 23%. This scatter is, statistically speaking, fully accounted for by the scatter of experimental permeabilities caused by the inhomogeneity of the samples.

The various assumptions made in the model also might result both in a random scatter and in the systematic deviation of the values obtained by the model, that is, Equation (33).

The assumption of circular cross section of the capillary segments might be a serious source of error were it not for the at least partial cancellation of this effect for the crucial diameters of the entry pores which were calculated from capillary pressure data by using the very same assumption (Carman, 1956).

As it was pointed out by Scheidegger (1963), the permeability equations obtained by him for the parallel and serial type capillaric models were extremely sensitive to the serious errors which usually exist at the two extremities of the pore size distribution curve. For the present permeability model, however, this is not the case as the greatest contribution to k_m comes from those k_i's that correspond to the neighborhood of the peak of the mercury porosimetry curve which is the best defined part of the distribution. The two extremities of the mercury porosimetry curve contribute only negligibly to the value of k_m.

The assumption of the Hagen-Poiseuille equation in the model implies that dissipation of the mechanical energy owing to curvatures and to convergent-divergent flow was neglected in the model. It has been shown by the experiments of Dullien and Azzam (1973) that, at least for short pieces of cylindrical capillaries of different diameter, fitted end-to-end, this dissipation effect may be significant. Allowing for these effects in the model would have resulted in lower permeabilities k_m.

There is another source of error in the model calculations which is due to the assumption that all the fluid contained in the volume elements V_{ij} is flowing when under the influence of a pressure gradient. These volumes, however, have been determined by mercury porosimetry, and it is likely that not all of the mercury which is injected into

the evacuated sample at a certain capillary pressure forms continuous arteries. Some of the mercury may be contained in capillaries which branch off from the arteries and contain narrow necks at certain points, preventing further penetration of the mercury under the given capillary pressure. Evidently when imposing a pressure gradient, only the mercury contained in the continuous arteries will flow whereas the mercury contained in the pseudo dead-end branch capillaries will not. Therefore, in the model calculations the values of V_{ij} used for the biggest value of i (that is to say, the largest entry pores) were presumably too big resulting in excessively large values k_i. By the same token the k_i of the channels with the smallest pore entry diameter (lowest value of i) might have been underestimated, but on the balance it is reasonable to expect that the predicted permeability k_m would turn out to be less if there had been a way to allocate the effective pore volumes more accurately to the different classes i of flow channels.

Summing up, it seems certain that if the present model were perfected by eliminating or at least decreasing the above sources of error unaccounted for in the present calculations, the result would be a decrease in the predicted permeability value k_m.

ACKNOWLEDGMENTS

Thanks are due first of all to Professor H. Rumpf of the Universität Karlsruhe whose gracious hospitality the author enjoyed as Visiting Professor while writing this paper. The many stimulating discussions initiated by participants of a series of post graduate seminars conducted by the author at Universität Karlsruhe have been most helpful in clarifying certain important points. Special thanks are due to Dr.-Ing. H. P. Kurz for pointing out to the author that the diagonal permeability of a square lattice has the same value as the permeabilities in the principal directions. A Travel Grant by the National Research of Canada is gratefully acknowledged.

NOTATION

A = cross-sectional area perpendicular to direction of macroscopic flow
a = cell constant
D = pore diameter
k = permeability
k_0 = shape factor
k' = Kozeny constant, $[k_0 (L_e/L)^2]$
L = length of macroscopic flow path
L_e = average, effective length of microscopic flow paths along L
l_{ij} = length of a pore segment
l_i = capillary length in the i-cell
n_{ij} = number of l_{ij} segments in the model
n = number of capillaries in the i-cell
P = pressure
Q = volumetric flow rate
S = specific surface area based on solids volume
V = volume
x = ratio of large-to-small diameter (D_l/D_s)
y = number ratio of large-to-small capillaries (ν_l/ν_s)
y = length ratio of large-to-small capillaries (l_l/l_s)

Greek Letters

$\alpha(D_e, D)$ = bivariate pore size distribution function
α = angle defining orientation of plane perpendicular to macroscopic flow direction
$\beta(D, D_e)$ = size distribution of pores the entry to which is controlled by necks greater than or equal to D_e
β = angle defining orientation of plane perpendicular to macroscopic flow direction
ϵ = bulk porosity
μ = viscosity

Subscripts

CK denotes Carman-Kozeny permeability
e denotes entry pore
H denotes hydraulic diameter
i = dummy index referring to size of narrowest segment (entry pore) in a flow capillary
j = dummy index referring to size of a segment in a flow capillary
l = large
m denotes model permeability
s = small
x denotes x-coordinate direction
y denotes y-coordinate direction
z denotes z-coordinate direction

LITERATURE CITED

Azzam, M. I. S., "Experimental and Theoretical Study of the Volume Averaged Navier-Stokes Equation in Porous Media," Ph.D. thesis, University of Waterloo (1974) (in preparation).

Batra, V. K., "An Experimental Investigation of the Structure of Porous Media and its Relation to Oil Recovery," Ph.D. thesis, University of Waterloo (1973).

Bear, J., *Dynamics of Fluids in Porous Media,* American Elsevier, New York, London, Amsterdam (1972).

Carman, P. C., *Flow of Gases through Porous Media,* Butterworths, London (1956).

Childs, E. C., and N. Collis-George, "The Permeability of Porous Materials," *Proc. Royal Soc.*, **A. 201,** 312 (1950).

Dhawan, G. K., "Photomicrographic Investigation of the Structure of Sandstones and other Porous Media by the Methods of Quantitative Stereology: With Application to Oil Recovery," Ph.D. thesis, University of Waterloo, Ontario (1972).

Dullien, F. A. L., and M. I. S. Azzam, "Flow Rate-Pressure Gradient Measurements in Periodically Non-Uniform Capillary Tubes," *AIChE J.*, **19,** 222 (1973).

Dullien, F. A. L., and V. K. Batra, "Determination of the Structure of Porous Media," *Ind. Eng. Chem.*, **62,** 25 (1970).

Dullien, F. A. L., and G. K. Dhawan, "Photomicrographic Size Distribution Determination of Non-Spherical Objects," *Powder Technol.*, **7,** 305 (1973).

———., "Characterization of Pore Structure by a Combination of Quantitative Photomicrography and Mercury Porosimetry," *J. Interface Colloid Sci.*, **47,** 337 (1974).

———., "Bivariate Pore Size Distributions of Some Sandstones," *J. Interface Colloid Sci.*, in press.

Dullien, F. A. L., and P. N. Mehta, "Particle Size and Pore (Void) Size Distribution Determination by Photomicrographic Methods," *Powder Technol.*, **5,** 179 (1971/72).

Dullien, F. A. L., "Use of Three-Dimensional Networks to Model Permeabilities of Porous Media," to be published.

Haines, W. B., *J. Agr. Sci.*, **20,** 97 (1930).

Hewitt, G. F., *Porous Carbon Solids,* R. L. Bond (ed.), p. 203 Academic Press, London (1967).

Kyan, C. P., D. T. Wasan, and R. C. Kintner, "Flow of Single-Phase Fluids through Fibrous Beds," *Ind. Eng. Chem. Fundamentals,* **9,** 596 (1970).

Rumpf, H., and A. R. Gupte, "Einflüsse der Porosität und Korngrössenverteilung im Widerstandsgesetz der Porenströmung," *Chem.-Ing.-Techn.*, **43,** 367 (1971).

Satterfield, C. N., *Mass Transfer in Heterogeneous Catalysis,* M.I.T. Press, Cambridge, Mass. (1970).

Scheidegger, A. E., "The Physics of Flow through Porous Media," Univ. Toronto Press (1963).

Schubert, H., "Untersuchungen zur Ermittlung von Kapillardruck und Zugfestigkeit von feuchten Haufwerken aus körnigen Stoffen," Doktor-Ing. dissertation, Universität Karlsruhe, Germany (1972).

Smith, W. O., "Capillary Flow through an Ideal Uniform Soil," *Physics,* **3,** 139 (1932).

Manuscript received July 23, 1974; revision received November 12 and accepted November 13, 1974.